Electronic Supplementary Material (ESI) for ChemComm.
This journal is © The Royal Society of Chemistry 2020

Complete Denitrification of Nitrate and Nitrite to N_2 gas by Samarium(II) Iodide

Walker R. Marks†, Douglas F. Baumgardner†, Eric W. Reinheimer‡, and John D. Gilbertson†

†Department of Chemistry, Western Washington University, Bellingham, Washington 98825, United States

‡Rigaku Oxford Diffraction, Woodlands TX 77381, United States

Table of Contents **Page**

General Methods

All reagents were purchased from commercial sources. Solvents were dried using a PureSolv solvent purification system and degassed by freeze-pump-thaw. Nano-pure water was generated by a Millipore Mili-Q Advantage A-10 nano-pure system. Nitrous oxide (N_2O) was purchased from AirGas, inc. and passed through an OxyClear deoxygenation and drying column before use. Nitric oxide (NO) was purchased from Praxair, inc. and used as received with no further purification. SmI_2 THF solution was purchased from either Sigma-Aldrich or Strem Chemicals, concentrations were checked via UV-Vis monitoring the absorbance at 618 nm with a published molar absorptivity of 877 L mol^{-1} cm^{-1}.[1] Gases were delivered by means of Hamilton gas-tight syringe through a suba-seal #25 septa. Reactions were carried out either inside of an argon-filled glovebox or by first freeze-pump-thawing the reaction solution before the addition of gaseous reagents. Infrared spectra were collected on a Thermo Scientific Nicolet iS10 FT-IR spectrometer using a transmission attachment and a PIKE Technologies 100 mm short-path gas IR cell with 36 mm NaCl windows. IR spectra were collected by evacuating a gas transmission IR cell and sampling through the septa of the reaction flask. Resolution was set to 0.5 cm^{-1} with 64 scans. UV-Vis spectra were collected on a JASCO V-670 spectrometer at room temperature in 1 cm quartz cuvettes (Starna Cells). Gas chromatography was conducted on an SRI 8610C GC with a thermal conductivity detector (TCD) utilizing argon as the carrier gas equipped with an Agilent Carboxen-1000 column. Ion chromatography (IC) was conducted with an Agilent 1100 Series HPLC with a simple anion column and a Waters 432 conductivity detector. Crystal data was collected with a Rigaku XtaLab Pro XRD using a Mo source at 80 K. Mass spectrometry was carried out using an Advion CMS expression^L mass spectrometer.

NO_x^- Reductions

All reactions were set-up in an argon-filled glovebox using 25 mL air-free side-arm flasks with PTFE stoppers and a suba-seal #25 septa. To an oven dried flask was added a PTFE stir-bar and either $NaNO_2$ or KNO_3 according to the desired molar ratio adjusted for the concentration of the SmI_2 solution verified by UV-Vis. The stopper was then screwed into the flask to allow liquid to flow down the arm while not allowing gases to escape the system. Using a large syringe, 10 mL of headspace was removed from the flask and then quickly replaced with 10 mL of Sm(II) I_2 THF solution. Once the solution was added the PTFE stopper was closed tightly and the reaction was allowed to stir for 48 hours at ambient temperature.

Nitrous Oxide (N_2O) Reduction

To an oven dried 25 mL air-free side-arm flask charged with a PTFE stir bar 5 mL of SmI_2 solution in THF was added. The vessel was sealed with a PTFE stopper and the sidearm sealed with a suba-seal #25 septa. The solution was then degassed by three consecutive rounds of freeze pump thaw. N_2O (one or two mole equivalent relative to SmI_2, concentration verified via UV-Vis spectroscopy) was then layered onto the frozen THF at 77 K. The vessel was then

allowed to warm and stir for two days at ambient temperature after which the solution had turned from deep blue to pale yellow.

Nitric Oxide (NO) Reduction

To an oven dried 25 mL air-free side-arm flask charged with a PTFE stir bar 5 mL of SmI_2 solution in THF was added. The vessel was sealed with a PTFE plug and the sidearm sealed with a suba-seal #25 septa. The solution was then degassed by three consecutive rounds of freeze pump thaw. Nitric oxide (one or two mole equivalent relative to SmI_2, concentration verified via UV-Vis spectroscopy) was then injected into the system. The vessel was then stirred at ambient temperature for three days after which the solution had turned from deep blue to pale yellow.

UV-vis

After the reactions were complete, 100 µL of the reaction solution was added to THF to a final volume of 10 mL. Spectra were collected with both a THF baseline and dark correction at a scan rate of 400 nm min^{-1} with a near IR resolution of 4 nm and ultraviolet-visible resolution of 2 nm, sampled every 1 nm.

Ion Chromatography

Once NO_x^- reduction was complete, after 48 hours of stirring, the reaction solvent was removed under reduced pressure. The resultant solid was then dissolved into 100 mL of nano-pure water. 1 mL of this solution was then added to nano-pure water to a total volume to 10 mL. The solution was then passed through a 0.22 µm, polypropylene membrane, syringe filter. Calibration was conducted using external standards made from $NaNO_2$ or KNO_3 in nano-pure water. Ion retention times (in minutes) are as follows; F^-: 1.81, Cl^-: 2.51, NO_2^-: 3.02, NO_3^-: 3.98, SO_4^-: 6.25, I^-: 7.45.

Gas Chromatography

Reaction headspaces were collected after 48 hours of reaction time using a Hamilton 2.5 mL gas-tight syringe. To sample the headspace the reaction flask stopper was opened and allowed to equilibrate for several minutes before piercing the septa and sampling 500 µL. GC calibration was done by flushing a vial of the same volume as the reaction headspace with argon, then injecting known quantities of analyte using a gas-tight syringe and allowing the vial to equilibrate for 30 minutes before sampling 500 µL. The temperature profile for all GC runs was 30° C for 8 min, then ramp at 20° C min^{-1} until temperature is 200° C, finally hold for 12 min. GC traces were plotted as a difference plot of the background and signal area as determined by PeakSimple software (SRI Instruments). The hydrogen signal present in some of the GC traces has been attributed to adventitious water. Regardless, the hydrogen signal is overrepresented due to the appreciably higher thermal conductivity of hydrogen (186.9 mW/m/K @300K) over the carrier gas, argon (17.9 mW/m/K @300K). Hydrogen signals for all reactions accounts for $\leq$ 1 mol% SmI_2 consumption. Retention times (in minutes) are as follows; H_2: 1.5, O_2: 5.3, N_2: 5.6, NO: 7.2, N_2O: 21.2.

Mass Spectrometry

Preparation of MS samples was done by removing all reaction solvent, then making an approximately 1 mM MeCN solution based on the initial concentration of samarium. MS spectra were collected using an Advion CMS expression^{L} mass spectrometer. Samples were prepared in MeCN and directly infused into the mass spectrometer using MeCN as a carrier at 0.3 mL/min. Data was analyzed using Advion Data Express software package.

Iodine Titration

A 22.4 mM solution of sodium thiosulfate was prepared in deionized water and loaded into a burette. The THF reaction solution was added to 90 mL deionized water with three rinses of the reaction vessel with deionized water and stirred vigorously for about 30 seconds. To the reaction solution was added 3 mL starch indicator solution in deionized water causing the solution to take on an almost black, purple-blue color. The solution was titrated with the sodium thiosulfate solution with strong stirring until the solution turned colorless, the endpoint.

Synthesis

Synthesis of $[SmI_2(THF)_5][SmI_4(THF)_2]$ (**1**). The previously reported **1** was synthesized via a nitrous oxide reduction, as described above. The solution was filtered to remove any solid and the THF was allowed to evaporate yielding yellow crystals of **1** suitable for X-ray analysis.

Synthesis of $[Sm_6(\mu_3\text{-}OH)_8(\mu_6\text{-}O)(H_2O)_{24}][I_8]$ cluster (**2**)**.** The reaction solution of a nitrous oxide reduction, as described above, was evaporated under reduced pressure to dryness. The solid, assumed to be $[SmI_2(THF)_5][SmI_4(THF)_2]$ (0.63 g: 0.4 mmol) was then dissolved in approximately 20 mL of acetone. The acetone solution was allowed to evaporate on the bench-top resulting in the formation of yellow, hygroscopic crystals of **2** and a red-brown oil. The oil and crystals were loaded into a fine, glass fritted funnel and washed with 10 mL hexanes followed by 10 mL cold diethyl ether. Yield 28 % (0.28 g: 0.1 mmol). Combustion analysis of compound **2** was inconclusive given the nature of the solvent molecules and ligands present in the samples. However, numerous, separate syntheses yielded batches of crystals with the same X-ray structure/formula.

Synthesis of $[Sm_6(\mu_3\text{-}OH)_8(\mu_6\text{-}O)(CH_3CN)_2(H_2O)_{6.8}(C_3H_6O)_{11.2}][I_8]$ cluster (**3**)**.** The reaction solution of a nitrous oxide reduction, as described above, was evaporated under reduced pressure to dryness. Under an atmosphere of nitrogen, the solid was dissolved in 10 mL of a 25/25/50 mixture of tetrahydrofuran/acetonitrile/acetone. The solution was then filtered through celite and layered with an equal volume of pentane and left undisturbed for 2 days, yielding colorless, hygroscopic crystals of **3** suitable for X-ray crystallography. Combustion analysis of compound **3** was inconclusive given the nature of the solvent molecules and ligands present in the samples. However, numerous, separate syntheses yielded batches of crystals with the same X-ray structure/formula.

Crystallography

Data collections on yellow crystals of **1-3** were first undertaken by securing single crystals of each with dimensions of 0.53 x 0.38 x 0.15 mm^3, 0.48 x 0.37 x 0.24 mm^3, and 0.32 x 0.25 x 0.23 mm^3 respectively to Mitegen mounts using Paratone oil. Those crystals were then mounted on a Rigaku Oxford Diffraction (ROD) XtaLABPRO equipped with a Pilatus P200K hybrid photon counting (HPC) detector and fine-focused Mo $K_{\alpha 1}$ radiation (= 0.71073 Å). Reflection data was collected at 100 K with data collection strategies to ensure completeness and desired redundancy determined using CrysAlis^{Pro}.[2] Data processing for all samples was done using CrysAlis^{Pro} and included numerical absorption corrections applied via face-indexing using the SCALE3 ABSPACK scaling algorithm.[3] All structures were solved via intrinsic phasing methods using ShelXT and subjected to a least-squares refinement with ShelXL within the Olex2 graphical user interface.[4,5,6] The final structural refinement included anisotropic temperature factors on all constituent non-hydrogen atoms. Hydrogen atoms were attached via the riding model at calculated positions using suitable HFIX commands. Space groups were unambiguously verified by PLATON .[7]

The solid-state structure of **2** crystallized in the centrosymmetric, orthorhombic space group *Pnnm* and consists of one-quarter of the distorted octahedral cluster of trivalent samarium atoms, whose overall charge of +2 is balanced by iodide anions located on crystallographic special positions (I1 and I2) and general positions (I3). Like I1 and I2, the atoms Sm1, Sm2, Sm3, and O11 are all on special positions while those remaining in the asymmetric unit are on general positions. Even though it's on a crystallographic general position, I3 is disordered over two positions with the occupancy of each part set to 50%. The asymmetric unit also contains three interstitial water molecules: one was well-behaved while two others in the asymmetric unit were set to 50% occupancy to achieve reasonable thermal parameters.

Each of the samarium atoms is bound to triple-bridged oxygen atoms and a central oxygen atom. The coordination environment around each is Sm^{3+} completed by four coordinated water molecules, with one of the water molecules bound to Sm3 showing evidence of occupational disorder. The oxygen atom for this water molecule was split and the occupancies of the parts were freely-refined and hydrogen atoms attached using appropriate HFIX commands after completion of anisotropic refinement. For this disordered water molecule, hydrogen atoms were moved into reasonable positions after closer inspection of potential intermolecular contacts using the HIMP command. Their O-H bond distances were also fixed to 0.85 Å using the DFIX command.

Close inspection of the Sm-O distances within the cluster demonstrated slight differences. Those bonds between the three samarium atoms in the asymmetric unit and O11 (the central oxygen atom in the octahedaral cluster) were measured at 2.58401(8), 2.56579(5), and 2.56247(9) Å respectively while those between the samarium atoms and the triply-bridged oxygen atoms ranged from 2.37910(5) - 2.39786(4) Å. Successive least-squares refinement of the X-ray crystallographic data for **2** revealed peaks in the difference map suggestive of hydrogen atoms bound to the

bridging oxides yielding bridging hydroxides. As a direct result, the formula for the cluster with water molecules bound is $[Sm_6(\mu_3\text{-}OH)_8(\mu_6\text{-}O)(H_2O)_{24}]^{8+}$ with the charge balanced by 8 iodide anions.

For **3**, disorder within coordinated acetone molecules bound to samarium atoms was observed. This included a split occupancy on a lone coordination site of Sm1 involving acetone in two positions fixed to 60% occupancy and H_2O fixed to 40% occupancy. A second acetone bound to Sm1 showed no disorder. While all other coordinated acetone molecules showed signs of disorder, other coordinated H_2O and CH_3CN molecules bound to the Sm_6O_9 core showed no signs of disorder. All of the iodine anions within the asymmetric unit of **3** showed evidence of disorder. Two of the iodine anions had their occupancies freely-refined while the best thermal parameters from those remaining were achieved when the occupancies were set to 76:24 and 90:10. As a means to achieve reasonable bond distances and thermal parameters within the structural model for **3**, the SADI, SIMU, RIGU and EADP constraints and restraints were used while SIMU, RIGU, HIMP and DFIX were used for **2** and RIGU for **1**.

NMR

^{15}N NMR spectra were collected on a Bruker Avance III 500 MHz spectrometer at operating at 50.64 MHz (^{15}N). All spectra were referenced externally to neat nitromethane set to 0 ppm at 298 K in THF with the characteristic $^{15}N_2$ signal at -72 ppm.[8]

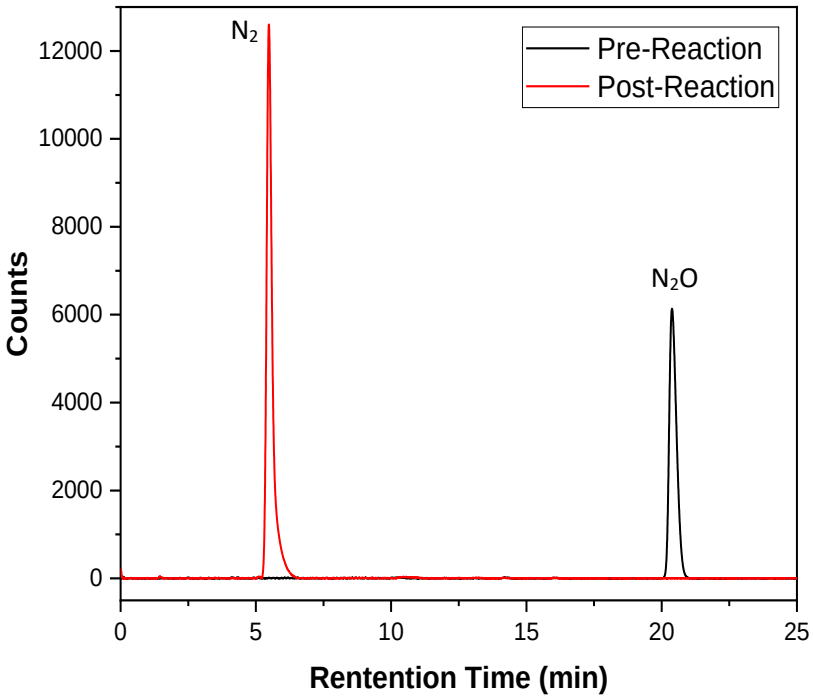

Figure S1. GC traces of before (black trace) and after (red trace) reduction of nitrous oxide (N_2O) (0.2 mmol) by 2 molar equivalents of samarium diiodide (0.4 mmol) showing complete conversion to dinitrogen.

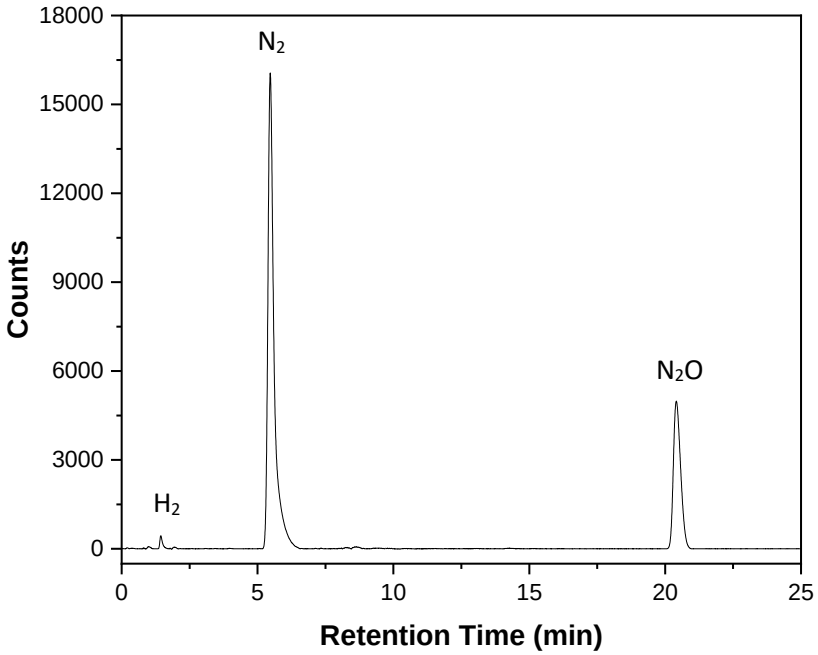

Figure S2. GC trace of the reduction of nitrous oxide (N_2O) (0.4 mmol) by 1 molar equivalent samarium diiodide (0.4 mmol) showing partial conversion to dinitrogen. The presence of hydrogen (< 1 mol% SmI_2) is attributed to adventitious water.

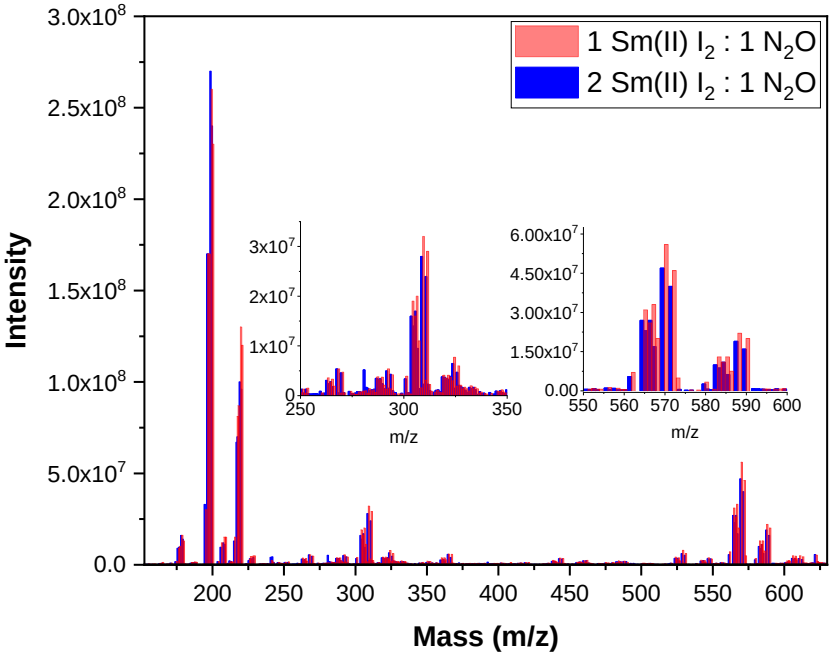

Figure S3. Mass spectra of the reduction of nitrous oxide (N_2O) by 1 molar equivalent samarium diiodide (0.4 mmol N_2O and 0.4 mmol SmI_2) (red trace) and 2 molar equivalents (0.2 mmol N_2O and 0.4 mmol SmI_2) (blue trace). Mass peaks of interest (m/z) 309: $[SmO(MeCN)_3(H_2O)]^+$, 569: $[SmI_2(MeCN)_4]^+$, 588: $[SmI_2(MeCN)_4(H_2O)]^+$.

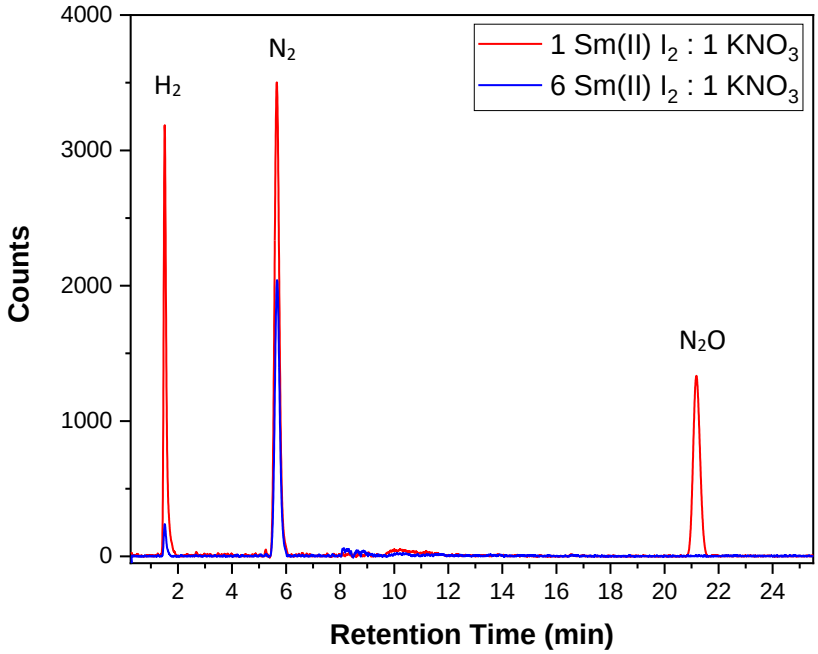

Figure S4. Gas chromatography traces of the reaction headspace after reduction of potassium nitrate by 1 molar equivalent samarium diiodide (0.8 mmol NO_3^- and 0.8 mmol SmI_2) in tetrahydrofuran (red trace) and 6 molar equivalents (0.13 mmol NO_3^- and 0.8 mmol SmI_2) (blue trace) respectively. The presence of hydrogen (< 1 mol% SmI_2) is attributed to adventitious water.

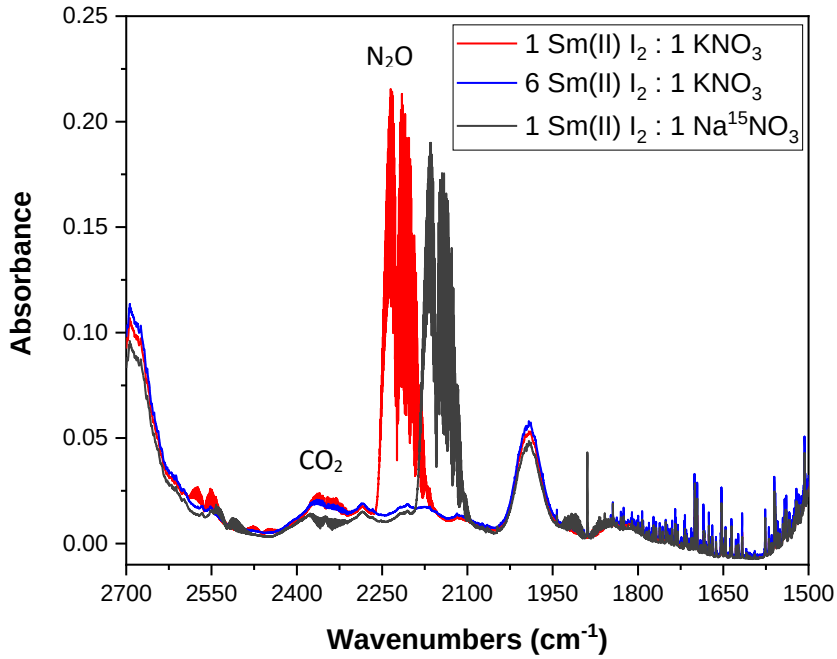

Figure S5. Gas-phase infrared absorption spectra of reaction headspace after reduction of potassium nitrate by 1 molar equivalent samarium diiodide in tetrahydrofuran (red trace) and 6 molar equivalents (red trace) respectively. Isotopic labeling with ^{15}N shown in black. CO_2 is from background.

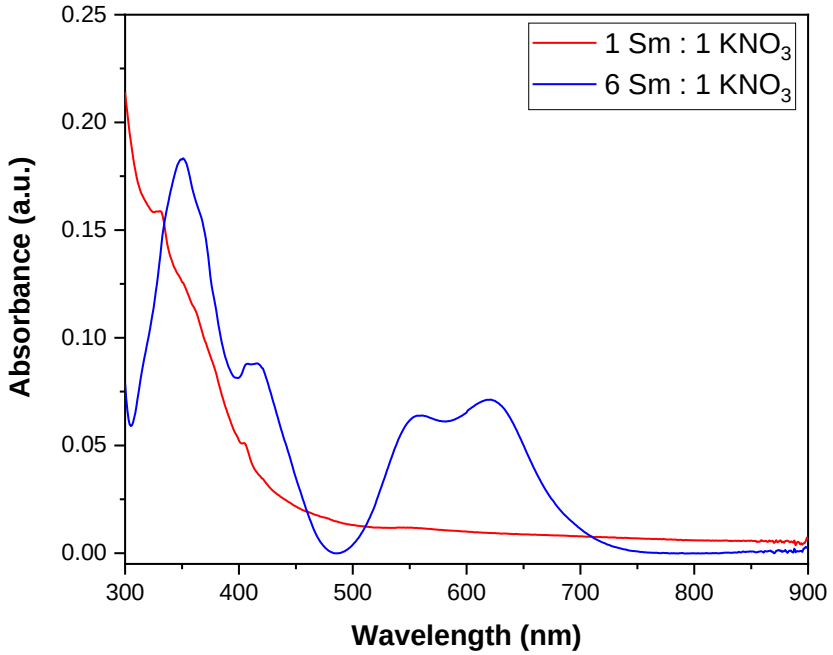

Figure S6. Ultraviolet-visible spectra of reaction solutions in tetrahydrofuran after reduction of potassium nitrate by samarium diiodide in tetrahydrofuran showing complete consumption of the samarium(II) when 1 molar equivalent SmI_2 is added to KNO_3 (0.8 mmol NO_3^- and 0.8 mmol SmI_2) (red trace) and incomplete consumption when 6 molar equivalents SmI_2 (0.13 mmol NO_3^- and 0.8 mmol SmI_2) (blue trace) are added.

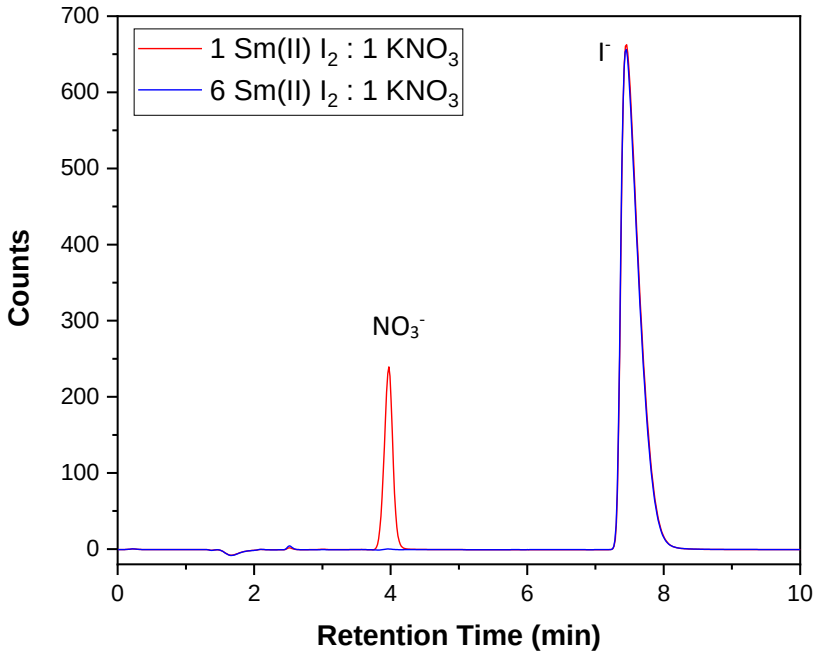

Figure S7. Ion chromatography traces in water of the reaction solution after reduction of potassium nitrate by 1 molar equivalent samarium diiodide (0.8 mmol NO_3^- and 0.8 mmol SmI_2) in tetrahydrofuran (red trace) or 6 molar equivalents (0.13 mmol NO_3^- and 0.8 mmol SmI_2) (blue trace) respectively.

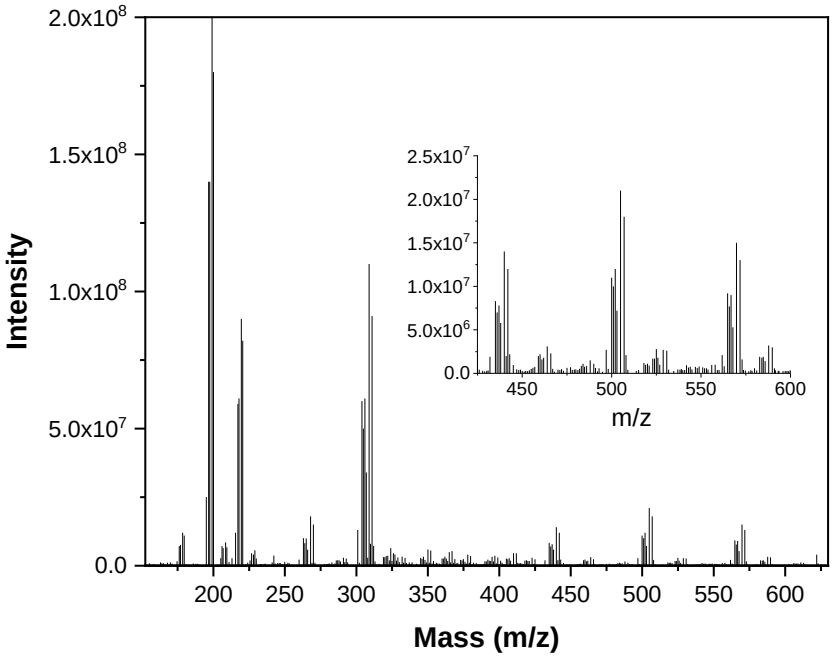

Figure S8. Mass spectrum of samarium diiodide reduction of potassium nitrate (0.8 mmol NO_3^- and 0.8 mmol SmI_2), 1 mM in acetonitrile. Mass peaks of interest (m/z) 309: $[SmO(MeCN)_3(H_2O)]^+$, 505: $[SmI_2(MeCN)_2(H_2O)]^+$, 569: $[SmI_2(MeCN)_4]^+$.

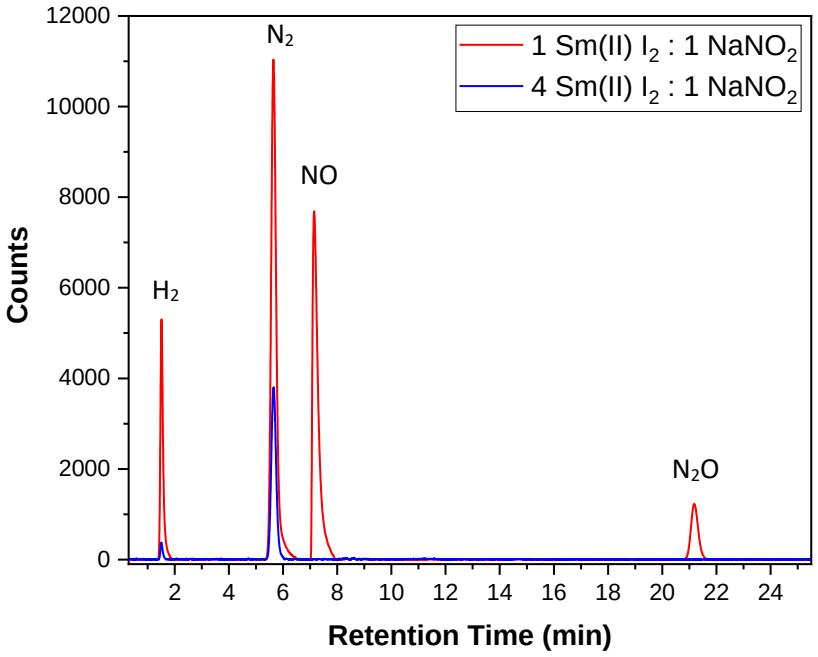

Figure S9. Gas chromatography traces of the reaction headspace after reduction of sodium nitrite by 1 molar equivalent samarium diiodide (0.8 mmol NO_2^- and 0.8 mmol SmI_2) in tetrahydrofuran (red trace) and 4 molar equivalents (0.2 mmol NO_2^- and 0.8 mmol SmI_2) (blue trace) respectively. The presence of hydrogen (< 1 mol% SmI_2) is attributed to adventitious water.

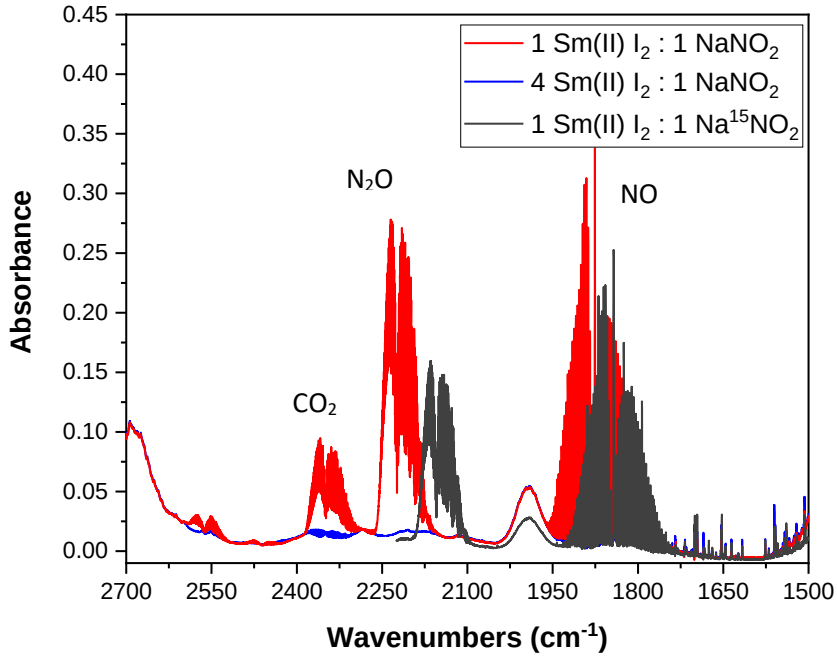

Figure S10. Gas-phase infrared absorption spectra of reaction headspace after reduction of sodium nitrite by 1 molar equivalent samarium diiodide in tetrahydrofuran (red trace) and 4 molar equivalents (red trace) respectively. Isotopic labeling with ^{15}N shown in black. CO_2 is from background.

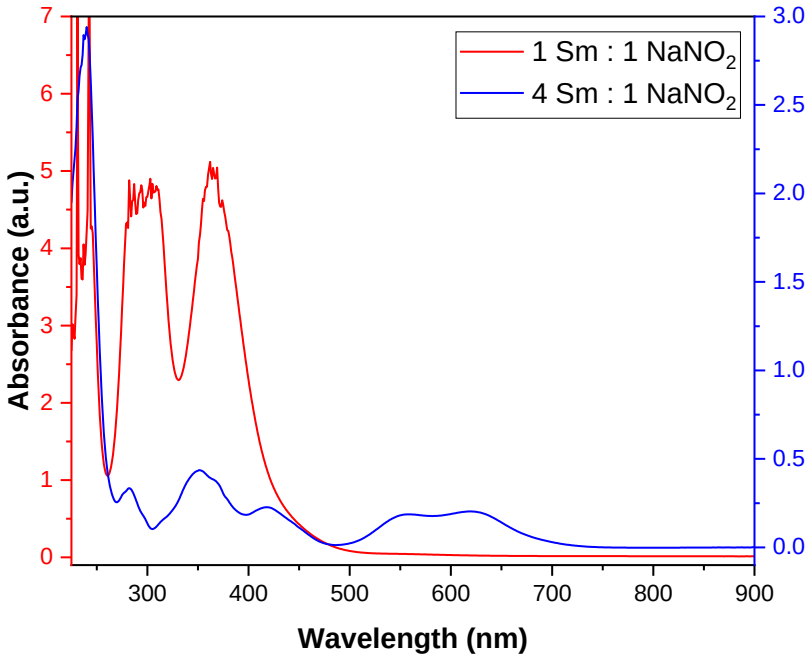

Figure S11. Ultraviolet-visible spectra of reaction solutions in tetrahydrofuran after reduction of sodium nitrite by samarium diiodide in tetrahydrofuran showing complete consumption of the samarium(II) when 1 molar equivalent SmI_2 is added to $NaNO_2$ (0.8 mmol NO_2^- and 0.8 mmol SmI_2) (red trace) and incomplete consumption when 4 molar equivalents SmI_2 (0.2 mmol $NO_2^-$and 0.8 mmol SmI_2) (blue trace) are added.

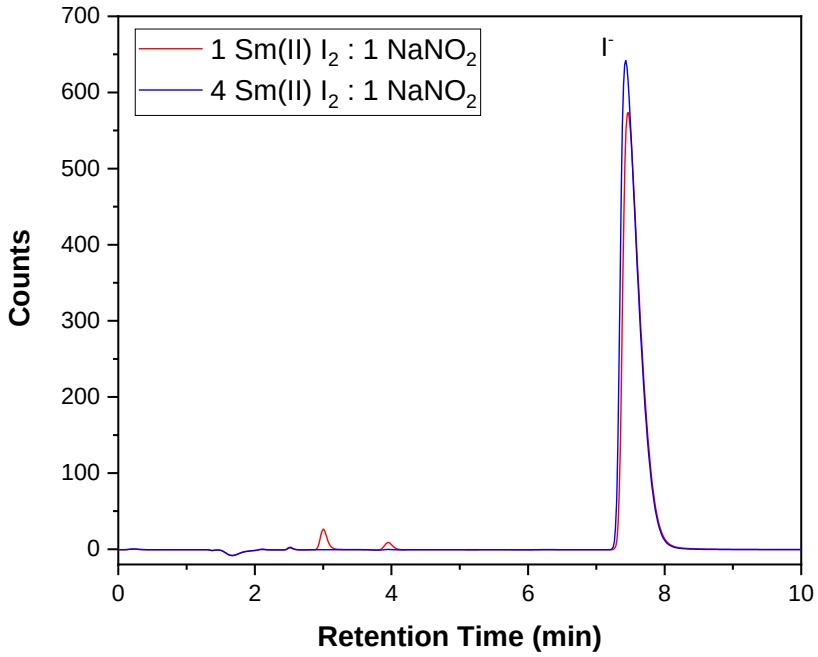

Figure S12. Ion chromatography traces of the reaction solution after reduction of Sodium Nitrite by 1 molar equivalent samarium diiodide (0.8 mmol NO_2^- and 0.8 mmol SmI_2) in tetrahydrofuran (red trace) or 4 molar equivalents (0.2 mmol NO_2^- and 0.8 mmol SmI_2) (blue trace) respectively.

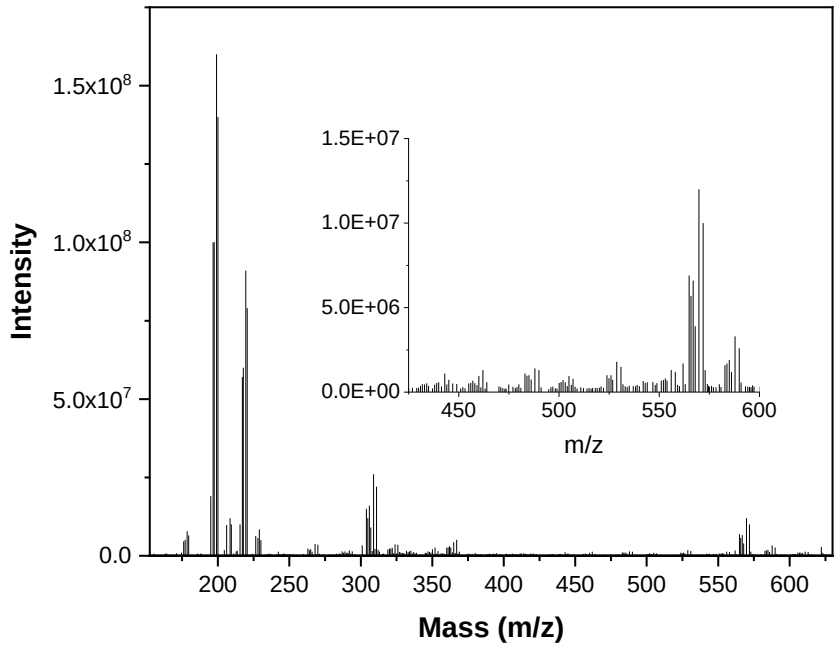

Figure S13. Mass spectrum of samarium diiodide reduction of sodium nitrite (0.8 mmol NO_2^- and 0.8 mmol SmI_2), 1 mM in acetonitrile. Mass peaks of interest (m/z) 309: $[SmO(MeCN)_3(H_2O)]^+$, 569: $[SmI_2(MeCN)_4]^+$, 588: $[SmI_2(MeCN)_4(H_2O)]^+$.

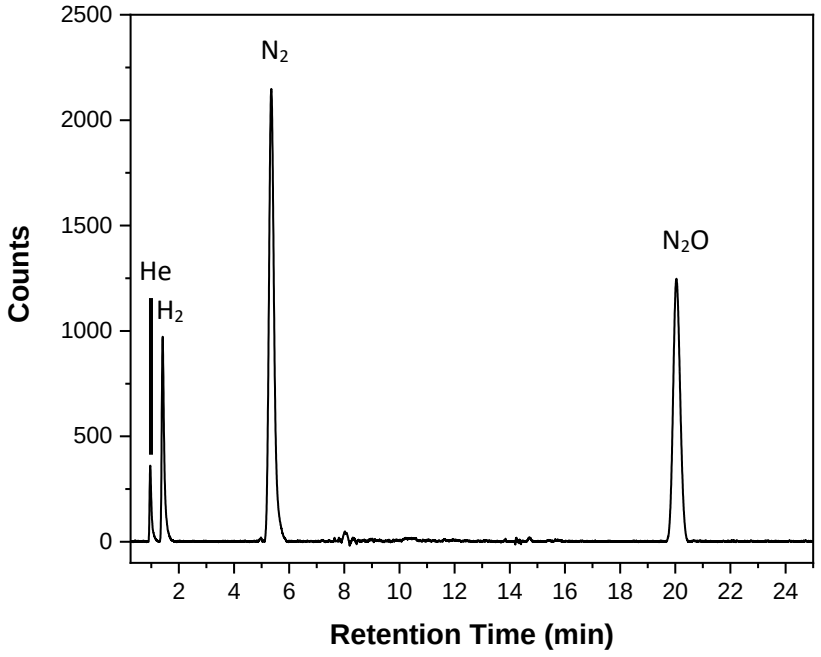

Figure S14. Gas chromatography traces of the reaction headspace after reduction of nitric oxide by 1 molar equivalent of samarium diiodide (0.4 mmol NO and 0.4 mmol SmI_2) in tetrahydrofuran. The presence of hydrogen (< 1 mol% SmI_2) is attributed to adventitious water, helium is present in the nitric oxide stock cylinder.

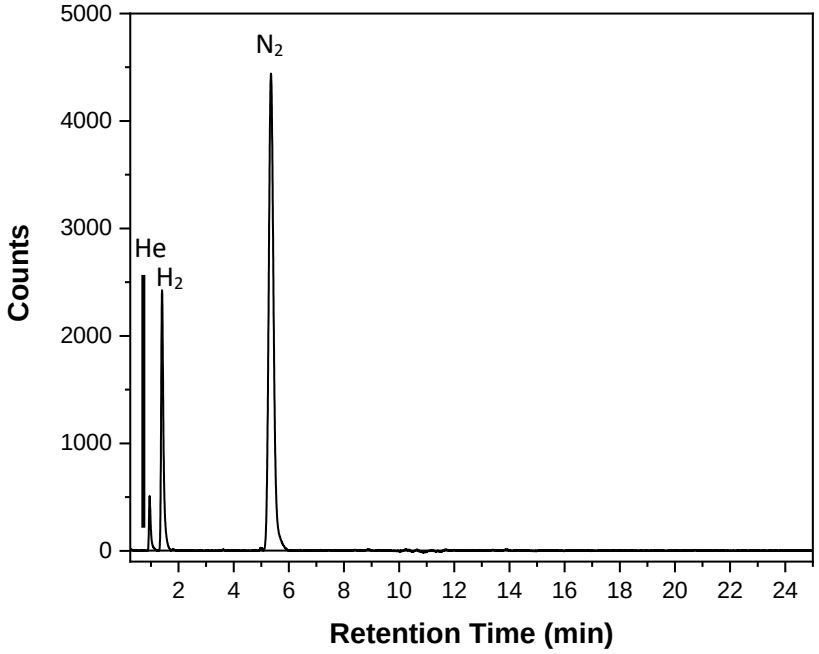

Figure S15. Gas chromatography traces of the reaction headspace after reduction of nitric oxide by 2 molar equivalents of samarium diiodide (0.2 mmol NO and 0.4 mmol SmI_2) in tetrahydrofuran. The presence of hydrogen (< 1 mol% SmI_2) is attributed to adventitious water, helium is present in the nitric oxide stock cylinder.

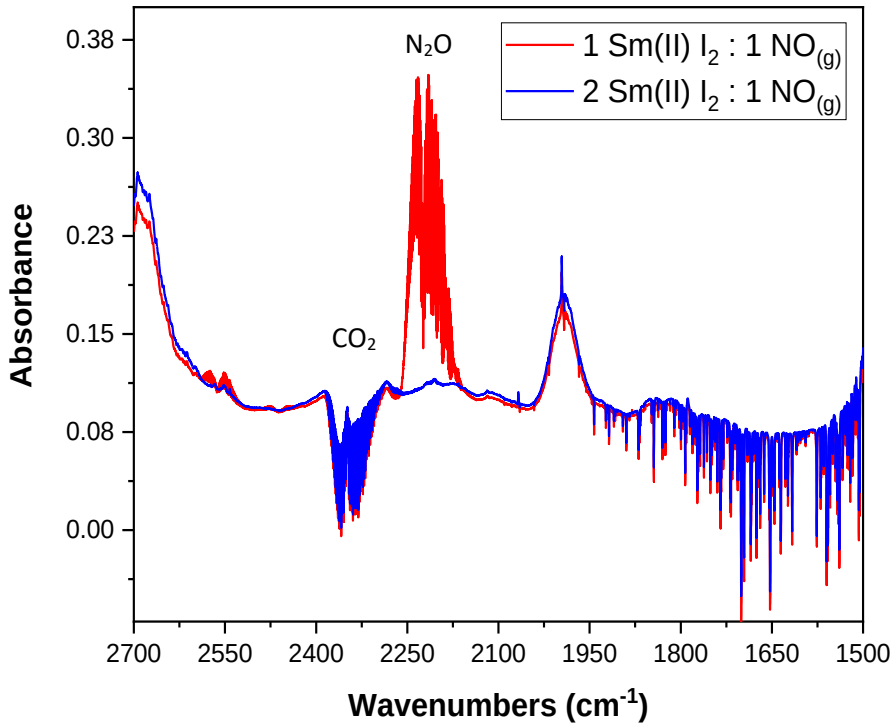

Figure S16. Gas-phase infrared absorption spectra showing the reduction of nitric oxide (NO) by samarium diiodide. Red spectrum shows complete reduction when an equimolar amount of NO is added (0.4 mmol NO and 0.4 mmol SmI_2) , the blue spectrum shows complete consumption of the resultant nitrous oxide (N_2O) when 0.5 molar equivalents of NO is added (0.2 mmol NO and 0.4 mmol SmI_2) . Carbon dioxide is due to an imperfect background correction.

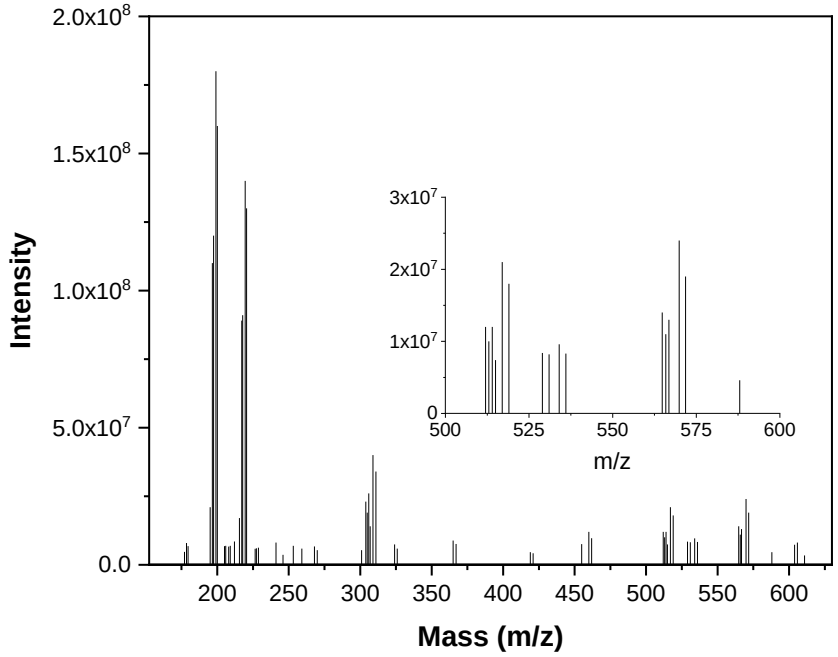

Figure S17. Mass spectrum of the oxidation of samarium diiodide by pure oxygen (0.4 mmol SmI_2 and excess O_2) , 1 mM in acetonitrile. Mass peaks of interest (m/z) 309: $[SmO(MeCN)_3(H_2O)]^+$, 569: $[SmI_2(MeCN)_4]^+$.

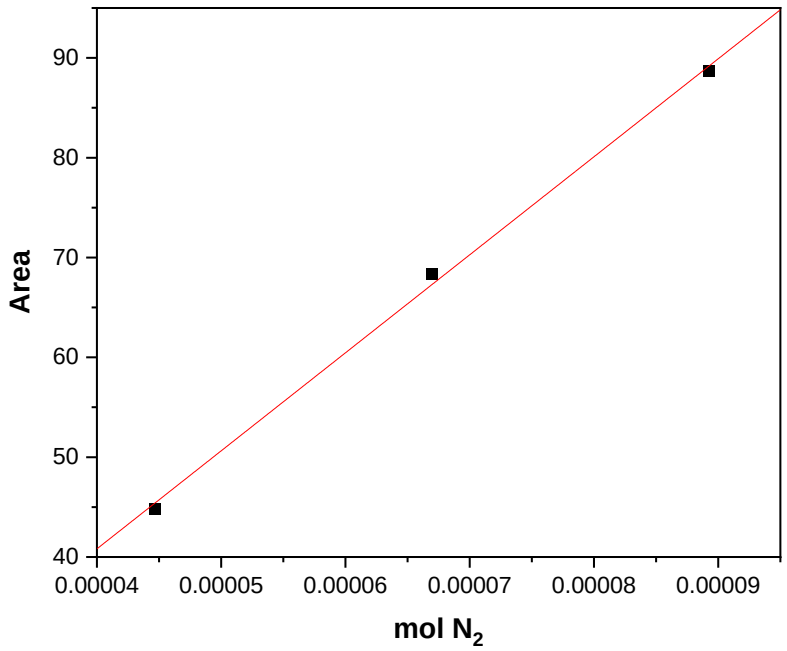

Figure S18. Dinitrogen calibration curve made by injecting N_2 into vials purged with argon. Linear fit parameters, slope: 981942.1, intercept: 1.5, R: 0.99914.

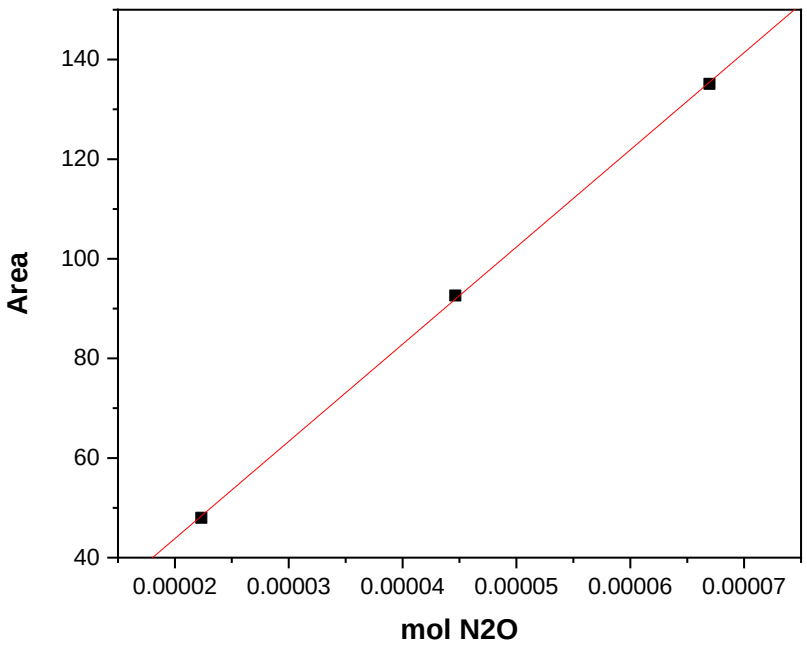

Figure S19. Nitrous oxide calibration curve made by injecting N_2O into vials purged with argon. Linear fit parameters, slope: 1.95E6, intercept: 4.814, R: 0.9996.

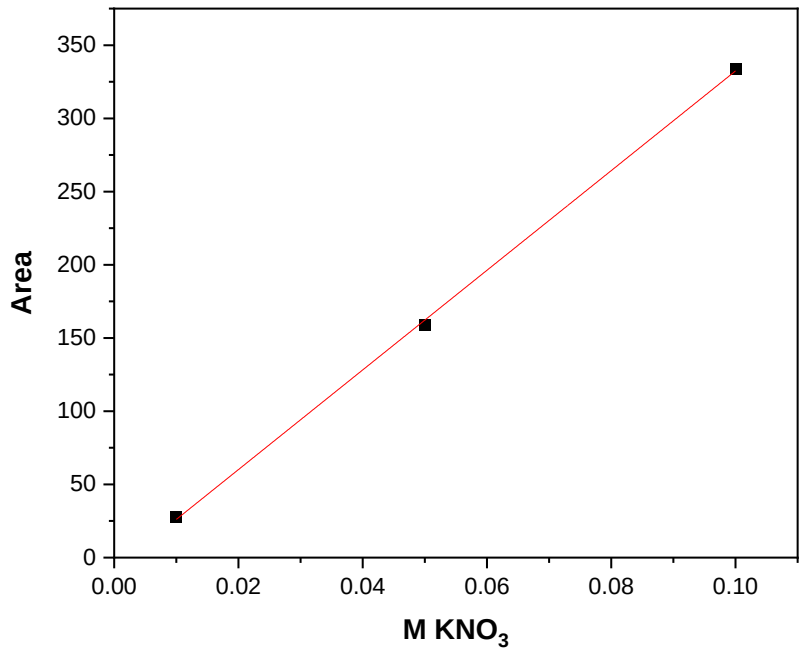

Figure S20. HPIC potassium nitrate calibration curve. Linear fit parameters, slope: 3403.5, intercept: -8.0, R: 0.99982.

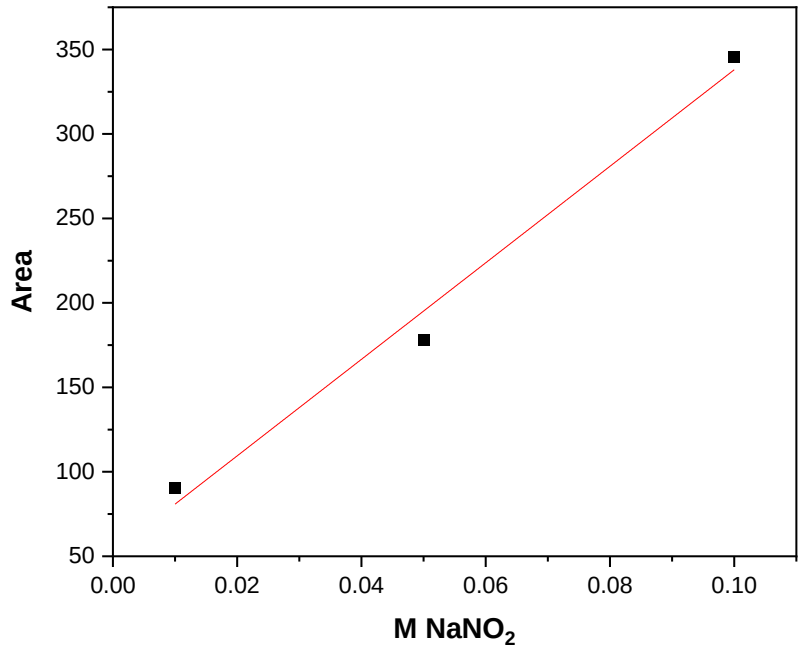

Figure S21. HPIC sodium nitrite calibration curve. Linear fit parameters, slope: 2857.1, intercept: 52.3, R: 0.99346.

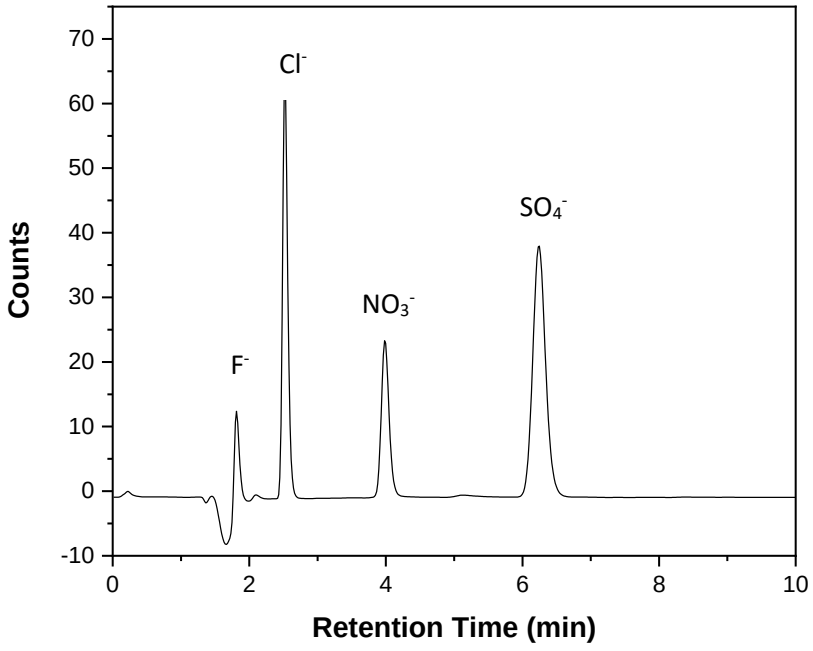

Figure S22. Ion chromatography standard of F^-, Cl^-, NO_3^-, and SO_4^- in nano-pure water.

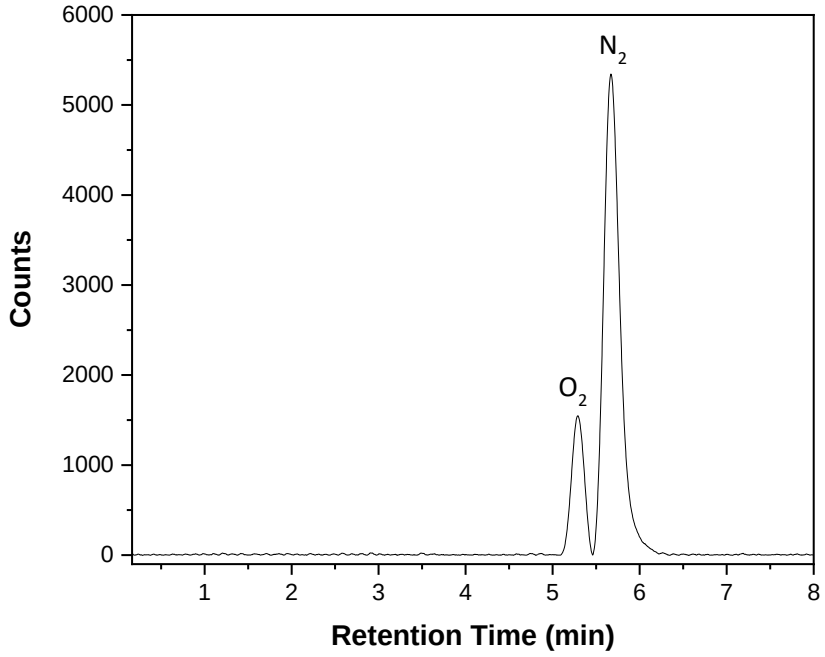

Figure S23. GC trace of air showing separation of oxygen and nitrogen.

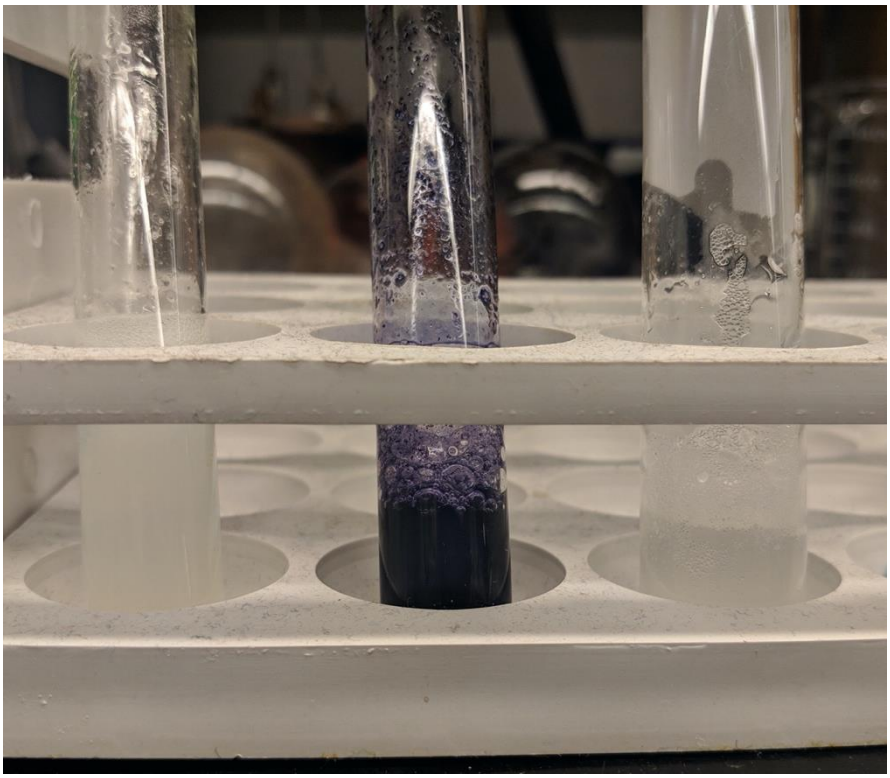

Figure S24. Starch test for iodine. 1 Nitrate : 1 samarium diiodide (left), 1 nitrite : 1 samarium diiodide (center), and sodium iodide blank (right). The purple color of the center reaction mixture indicates the presence of iodine while the colorless solutions show no iodine.

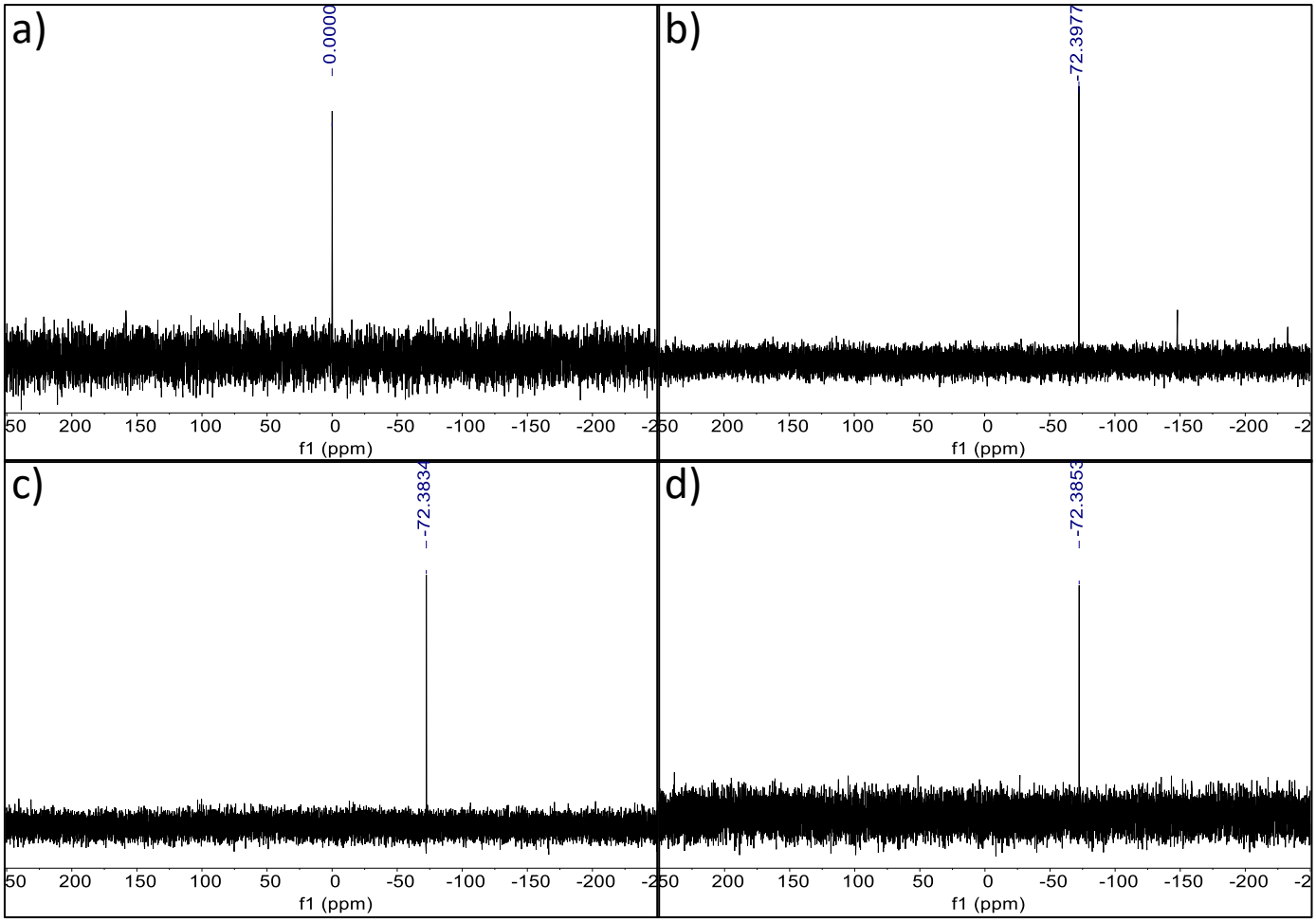

Figure S25. ^{15}N NMR spectra of a) neat nitromethane external reference, and reaction headspaces from b) reduction of Na^{15}NO$_3$ by 1 molar equivalent samarium diiodide, c) reduction of Na^{15}NO$_3$ by 6 molar equivalents samarium diiodide, and d) reduction of Na^{15}NO$_2$ by 4 molar equivalents samarium diiodide in THF.

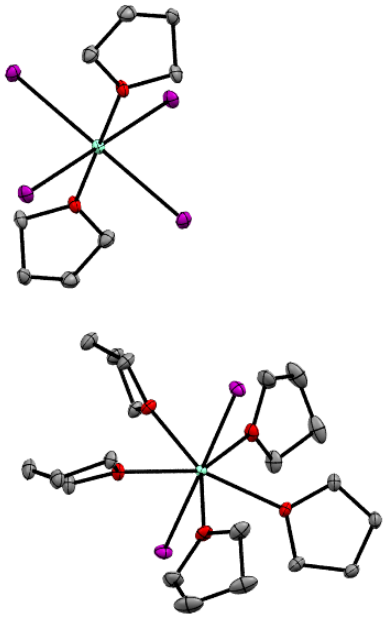

Figure S26. ORTEP view of $[SmI_2(THF)_5][SmI_4(THF)_2]$ (**1**). Thermal ellipsoids are shown at 50%.

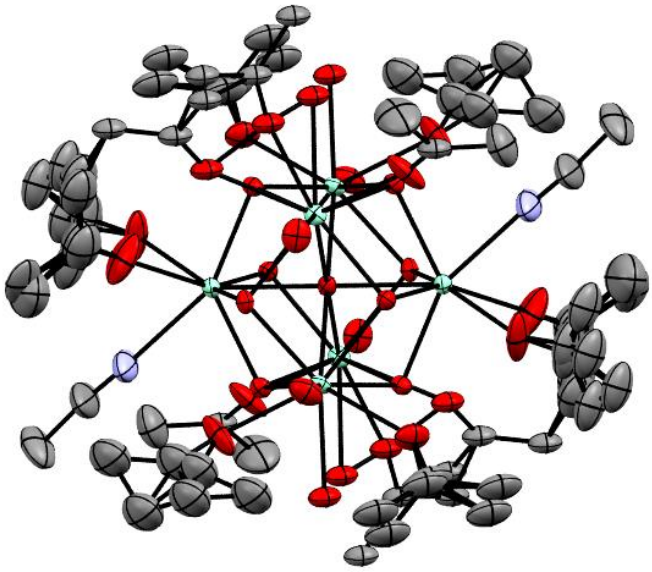

Figure S27. ORTEP view of $[Sm_6(\mu_3\text{-}OH)_8(\mu_6\text{-}O)(CH_3CN)_2(H_2O)_{6.8}(C_3H_6O)_{11.2}][I_8]$ (**3**) with hydrogen atoms and counter ions omitted for clarity. Thermal ellipsoids are shown at 50%.

Table S1. Selected bond lengths and angles for $[SmI_2(THF)_5][SmI_4(THF)_2]$ **(1).**

	Bond	Distance (Å)		Bond	Angle (°)
1	Sm(1)-I(1)	3.01988(14)	1	I(1)-Sm(1)-I(1')	179.13335(7)
2	Sm(1)-I(1')	3.01988(14)	2	O(1)-Sm(1)-O(2)	144.6036(9)
3	Sm(1)-O(1)	2.42523(12)	3	O(2)-Sm(1)-O(3)	71.7220(15)
4	Sm(1)-O(2)	2.44900(12)	4	O(3)-Sm(1)-O(2')	71.7220(15)
5	Sm(1)-O(3)	2.43005(12)	5	O(2')-Sm(1)-O(1')	144.6036(9)
6	Sm(1)-O(1')	2.42523(12)	6	O(1')-Sm(1)-O(1)	72.707(5)
7	Sm(1)-O(2')	2.44900(12)	7	O(1)-Sm(1)-I(1)	90.560(3)
8	Sm(2)-I(2)	3.04623(18)	8	O(3)-Sm(1)-I(1')	90.43332(4)
9	Sm(2)-I(3)	3.06475(16)	9	I(2)-Sm(2)-I(2')	180.00(5)
10	Sm(2)-I(2')	3.04623(18)	10	O(4)-Sm(2)-O(4')	180
11	Sm(2)-I(3')	3.06475(16)	11	I(3)-Sm(2)-I(3')	180
12	Sm(2)-O(4)	2.36968(11)	12	I(2)-Sm(2)-I(3')	91.610(4)
13	Sm(2)-O(4')	2.36968(11)	13	I(2')-Sm(2)-I(3)	91.610(4)
			14	I(2')-Sm(2)-I(3')	88.390(4)

Table S2. Selected bond lengths and angles for the $[Sm_6(\mu_6\text{-}O)(\mu_3\text{-}OH)_8][I_8]$ (**2**)

	Bond	Distance (Å)		Bond	Angle (°)
1	Sm(1)-O(4)	2.39786(4)	1	Sm(1)-O(4)-Sm(2)	99.695(2)
2	Sm(1)-O(8)	2.40047(4)	2	Sm(1)-O(4)-Sm(3)	98.8048(17)
3	Sm(1)-O(11)	2.58401(8)	3	Sm(1)-O(8)-Sm(3)	98.8972(15)
4	Sm(2)-O(4)	2.37910(5)	4	Sm(1)-O(11)-Sm(3)	90.000(6)
5	Sm(2)-O(8)	2.39010(4)	5	Sm(2)-O(4)-Sm(3)	98.8536(18)
6	Sm(2)-O(11)	2.56579(5)	6	Sm(2)-O(8)-Sm(3)	98.712(2)
7	Sm(3)-O(4)	2.39490(4)	7	Sm(2)-O(11)-Sm(3)	90.000(2)
8	Sm(3)-O(8)	2.38898(5)			
9	Sm(3)-O(11)	2.56247(9)			

Table S3. Selected bond lengths and angles for $[Sm_6(\mu_3\text{-}OH)_8(\mu_6\text{-}O)(CH_3CN)_2(H_2O)_{6.8}(C_3H_6O)_{11.2}][I_8]$.

	Bond	Distance (Å)		Bond	Angle (°)
1	Sm(1)-O(10)	2.37006(4)	1	Sm(1)-O(10)-Sm(2)	100.4179(19)
2	Sm(1)-O(12')	2.39633(4)	2	Sm(1)-O(10)-Sm(3)	97.0059(18)
3	Sm(1)-O(11')	2.39740(5)	3	Sm(1)-O(13)-Sm(3)	96.7161(18)
4	Sm(1)-O(13)	2.38483(5)	4	Sm(1)-O(14)-Sm(3)	89.7560(7)
5	Sm(1)-O(14)	2.55872(5)	5	Sm(2)-O(10)-Sm(3)	98.3149(14)
6	Sm(2)-O(10)	2.39605(4)	6	Sm(2)-O(11)-Sm(3)	98.2010(16)
7	Sm(2)-O(11)	2.40289(5)	7	Sm(2)-O(14)-Sm(3)	90.0510(4)
8	Sm(2)-O(13')	2.41128(4)			
9	Sm(2)-O(12')	2.41824(4)			
10	Sm(2)-O(14)	2.62279(7)			
11	Sm(3)-O(10)	2.38644(6)			
12	Sm(3)-O(13)	2.38237(5)			
13	Sm(3)-O(12)	2.37544(5)			
14	Sm(3)-O(11)	2.36724(5)			

References

1) J. A. Teprovich Jr., P. K. S. Antharjanam, E. Prasad, E. N. Pesciotta and R. A. Flowers II, *Eur. J. Inorg. Chem.*, *2008*, 5015–5019.
2) CrysAlisPro, Rigaku Oxford Diffraction, version 171.40.67a, 2019.
3) SCALE3 ABSPACK – A Rigaku Oxford Diffraction program for Absorption Corrections, Rigaku Oxford Diffraction, 2017.
4) G. M. Sheldrick *Acta Cryst*. *2015,* **A71**, 3-8.
5) G. M. Sheldrick *Acta Cryst*. *2015,* **C71**, 3-8.
6) O. V. Dolomanov, L. J. Bourhis, R. J. Gildea, J. A. K. Howard, H. Puschmann *J. Appl. Cryst*. *2009,* **42**, 339-341.
7) A.L.Spek, *Acta Cryst. 2009*, **D65**, 148-155.
8) Luck, I. J.; Li, H. L.; Hazari, N.; Field, L. D. *Magn. Reson. Chem.*, *2003*, **41**, 709-713.